SPECIAL PROJECT FINAL REPORT

All the following mandatory information needs to be provided.

Project Title:	Simulations with climate model EC-Earth
Computer Project Account:	spsezhan
Start Year - End Year :	2015 - 2017
Principal Investigator(s)	Qiong Zhang
Affiliation/Address:	Department of Physical Geography Stockholm University
Other Researchers (Name/Affiliation):	Qiang Li, Qiang Zhang

The following should cover the entire project duration.

Summary of project objectives
(10 lines max)

The project aims to setup the paleoclimate simulations with EC-Earth and perform various simulations for past climate. We have implemented the necessary components that specifically required for the paleoclimate and have done different simulations for the past climate, including five key periods suggested by PMIP (Paleoclimate Inter-comparison Project) and several project oriented sensitivity experiments (e.g. Green Sahara during mid-Holocene). The climate sensitivity has been evaluated under different climate forcing. Sensitivity experiments under these climate conditions have been performed to understand the mechanisms of past climate variability. The produced climate model data have been widely analysed for different scientific research questions within the collaboration.

Summary of problems encountered

In previous progress report we have described the problems we encountered with Last Glacial Maximum simulation. We have observed very large sea-ice thickness after 800 years simulation that can be 200 meters. We have not identified any reason that responsible for the thick sea-ice and speculate it may be due to the one-category of sea-ice in LIM3. This is mostly due to the sensitive sea-ice physics rather than the computation technique. Some small technical problems encountered during the last three years are usually solved quite quickly with the help from ECMWF technical support or EC-Earth technical support.

Experience with the Special Project framework
(Please let us know about your experience with administrative aspects like the application procedure, progress reporting etc.)

The experiences with application procedure and progress report are very good, I highly appreciate the remind sent from the system or administrative for the submission. Progress report is a nice way for us to check on the usage of the resources and to make better plan for the future work. The previous application needs to be sent through the member state National Meteorological Service, which I feel is not necessary. From this year the application can directly submitted online, much more efficient.

Summary of results
(This section should comprise up to 10 pages and can be replaced by a short summary plus an existing scientific report on the project.)

With the HPC support from ECMWF and NSC in Sweden, now we have established a model system that can well facilitate the paleo simulations. EC-Earth is international recognised as its higher resolution and good performance. We are invited to join several EU H2020 research proposals where require the multi-model participate. The below summary for the climate modelling works we have done with EC-Earth has been reflected in every year's progress report, now integrated in one report in the order of different experiments. We plan to document all the model implementation and paleo experiments setup in one paper and submit to *Geophysical Model Development*. For the unpublished work we provide a few figures for reference.

1. New implementations for paleo-component in EC-Earth

EC-Earth is built on the knowledge of present day and the physical parametrisations are based on present-day observation. However, we don't know if such a model is valid for another unknown climate condition, i.e. either a future scenario or climate in the past. When a climate model that developed for present-day is applied to a different climate condition, some new components need to
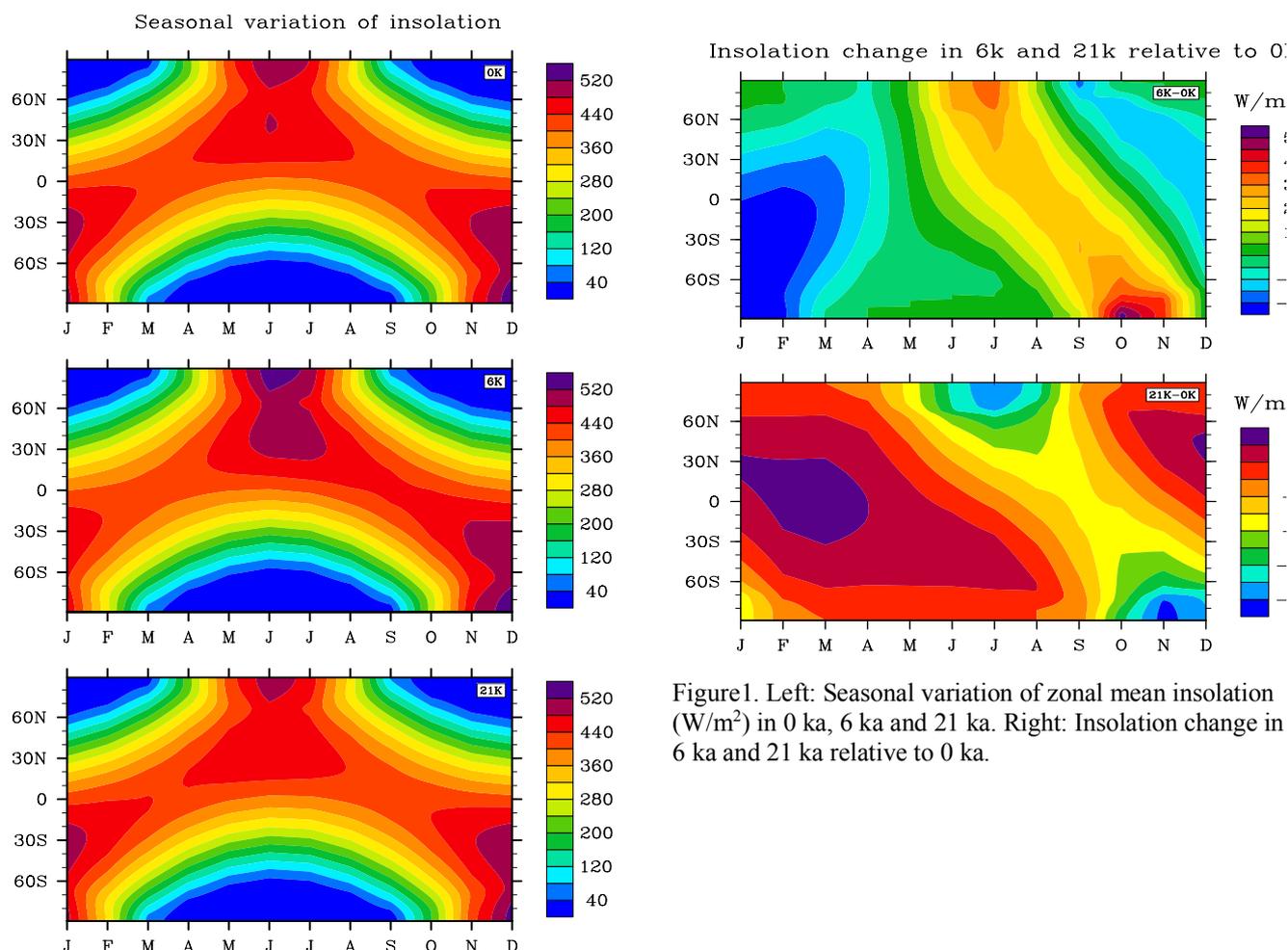
be implemented to facilitate the simulation for the past climate. For EC-Earth, we have done three implementations including the **orbital forcing**, **ice-sheet surface processes** and **Land surface albedo parametrization**.

1.1 Orbital forcing

Orbital forcing related parameters in IFS are treated as constants for the present-day climate; follow the recommendations of the International Astronomical Union (ARPEGE-Climate Version 5.1, 2008). It is noted that the formulas are not valid for dates too far away from the 1st January 2000 (more than one century). Therefore for paleoclimate simulations it is crucial to have the varied orbital parameters according to the given time.

New calculation for the orbital forcing is referred from CAM3.0. The below description for computing orbital parameters is adopted from NCAR technical note (2004) on "Description of the NCAR Community Atmosphere Model (CAM 3.0)", section 4.8 "Parameterization of Shortwave Radiation", with modifications that appropriate to IFS.

The insolation is computed using the method of Berger (1978). Using this formulation, the insolation can be determined for any time within 10 6 years of 1950 AD. This facilitates paleoclimate simulations. The formulation determines earth-sun distance factor and solar zenith angle. The annual and diurnal cycle of solar insolation are represented with a repeatable solar year of exactly 365 days and with a mean solar day of exactly 24 hours, respectively. The repeatable solar year does not allow for leap years.

Figure1. Left: Seasonal variation of zonal mean insolation (W/m^2) in 0 ka, 6 ka and 21 ka. Right: Insolation change in 6 ka and 21 ka relative to 0 ka.

The orbital state used to calculate the insolation is held fixed over the length of the model integration. This state may be specified in one of two ways. The first method is to specify a year. The value of the year is held constant for the entire length of the integration. The year must fall within the range of 1950 ± 10^6. The second method is to specify the orbital parameters: eccentricity,

longitude of perihelion, and obliquity. This set of values is sufficient to specify the complete orbital state. Settings for AMIP II style integrations under 1995 AD conditions are obliquity = 23.4441, eccentricity = 0.016715, and longitude of perihelion = 102.7.

We run the EC-Earth 3.0 (with configuration T159L62-ORCA1L46/LIM3) to test the new implemented orbital forcing. Model computes the orbital parameters according to the given year. Different orbital parameters will produce different insolation. In order to compare with the insolation from other models that use the same computation methods, we particularly run the test experiments for pre-industrial (0 ka,1850 AD), mid-Holocene (6 ka, 6000 BP) and Last Glacier Maximum (21 ka, 21000 BP) as shown in Figure 1. We compared the insolation with those from CESM and MPI-CSM provided by PMIP3 database and verified that the insolation from these three models is the same for 0 ka, 6ka and 21ka.

Figure1 also shows insolation change in mid-Holocene (6 ka) and LGM (21 ka) relative to pre-industrial, where demonstrating significant change in seasonality in 6 ka. Therefore the orbital forcing is regarded as the major forcing for mid-Holocene.

1.2 ice-sheet surface processes

Concerning the ice-sheet mass balance, the surface scheme (H-TESSEL) used in IFS does not treat ice sheet explicitly. The surface scheme models the ice sheet as 10m of perennial snow at which there is land ice and it is in thermal contact with the underlying soil. The albedo and density are fixed at 0.8 and 300 kg/m^3, respectively. In such setting, feedback process is not considered due to fixed parameters and problems of conservation of water exist since snow and ice-sheet melting are not allowed.
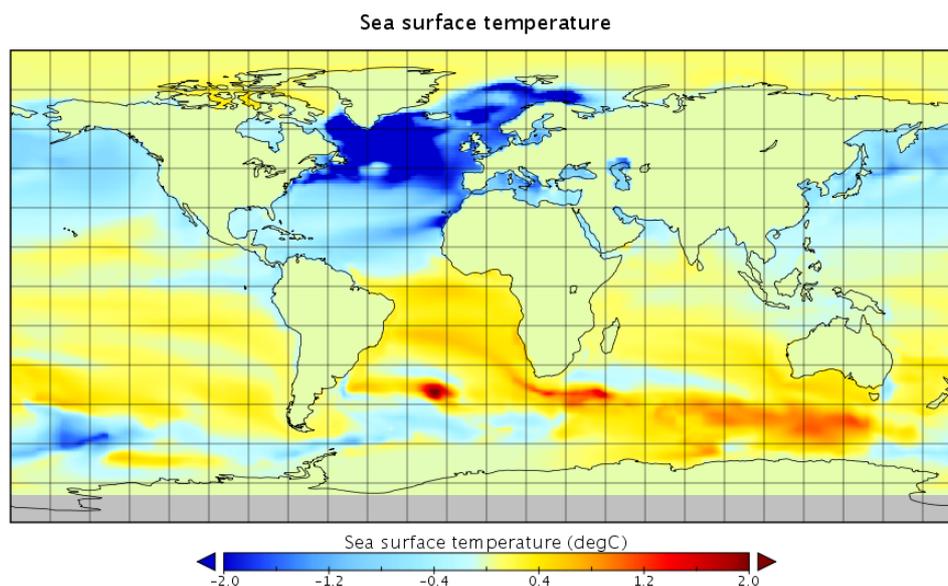

Figure 2. Global SST change between without and with ice-sheet surface process scheme for PI climate condition.

Therefore, a new surface process for the ice-sheet is introduced. The new land ice mask is applied on top of the original tiles. If a grid box is covered with at least 50% land ice, properties of soil like thermal conductivity and volumetric heat capacity are changed with those of ice as well as surface properties (i.e. albedo, long wave emissivity, roughness lengths for heat, momentum and moisture and skin layer conductivity) of land tiles not covered by snow (i.e. intercepted water, low/high vegetation and bare ground).

Snow is allowed to accumulate on ice sheets, but only with a net positive energy flux at the surface, the accumulated snow is allowed to melt under consideration of energy conservation. In the end, the melt snow will be redistributed to the ocean. Note that for the present setup which is not coupled to any ice-sheet model, all the melting only occurs on the surface, neither basal melt nor ice discharge is taken into account. In addition, a new albedo parametrization for snow on land ice is introduced.

The albedo is fixed at 0.8 for perennial snow while for seasonal snow, the albedo is set to 0.85 after snow fall and linearly decrease with ageing and exponentially decrease with melting with a minimum value of 0.6. Once the land-ice is not covered by the snow, it is also allowed to melt as long as the land ice coverage is larger than 10% and the skin temperature is greater than zero degree. This new surface process is adopted from previous work at DMI with EC-Earth 2.3. Therefore this implementation highly benefits from the collaboration with DMI, both from technical assistance and ECMWF computer resources sharing during the test stage.

The ice-sheet surface processes improved the cold biases in northern Hemisphere and warm biases in southern Hemisphere, as shown in Figure 2. The annual mean global averaged SST increased about 0.25C, which is closer to the observation.

1.3 Land surface albedo

One crucial forcing for the past climate is the land-use, this will lead to the change in the surface type and consequently changes of land surface albedo and surface energy balance. In current H-TESSEL the land-surface albedo is specified from MODIS 16-day albedo product (MOD43) over the year 2000-2003.
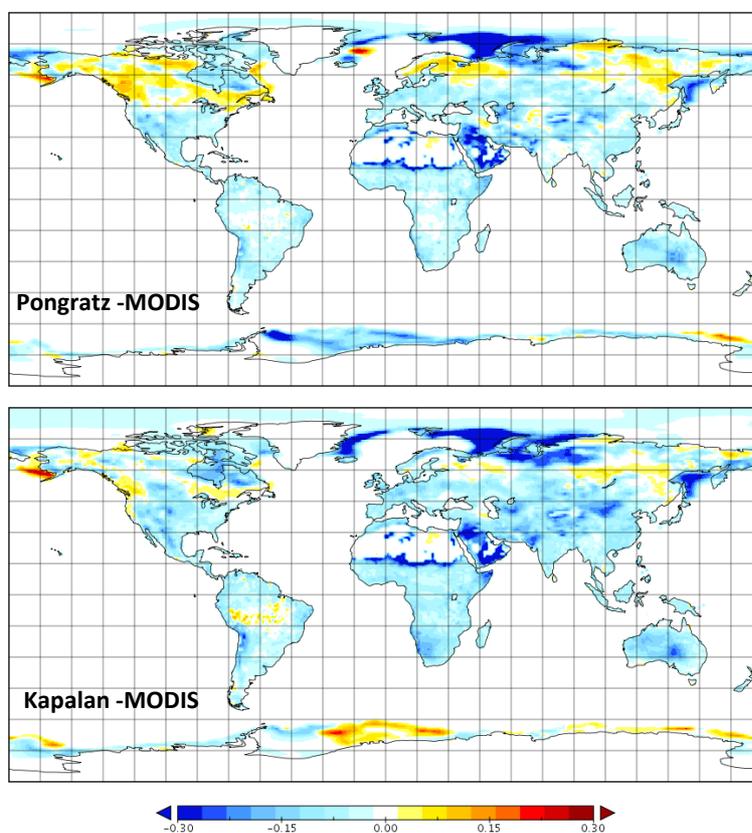

Figure 3. Difference between MODIS albedo and modified albedo according to land cover reconstruction for 1850AD, upper: Pongratz (2009); lower: Kapalan (2010).

Apparently for a different land surface type this albedo data should not held as fixed field. This is particularly important for our Last Millennium (LM) simulation setup where land-use is believed to vary significantly. PMIP protocol has provided two land cover reconstructions. In order to obtain a more realistic land-surface albedo, we have followed the calculations by Houldcroft et al (2009) to translate the modern MODIS albedo according to the land surface type. The land surface classification in H-TESSEL/EC-Earth and reconstructions are different, there are 20 vegetation types in H-TESSEL and 14 vegetation types in reconstructions. First, we have translated the 14 LM types to 20 BATS types that used in H-TESSEL. Houldcroft et al (2009) uses MODIS data to estimate the albedo of each cover type in which the classification of vegetation cover is based on IGBP classification scheme. We further translate BATS types to IGBP to calculate the land albedo.
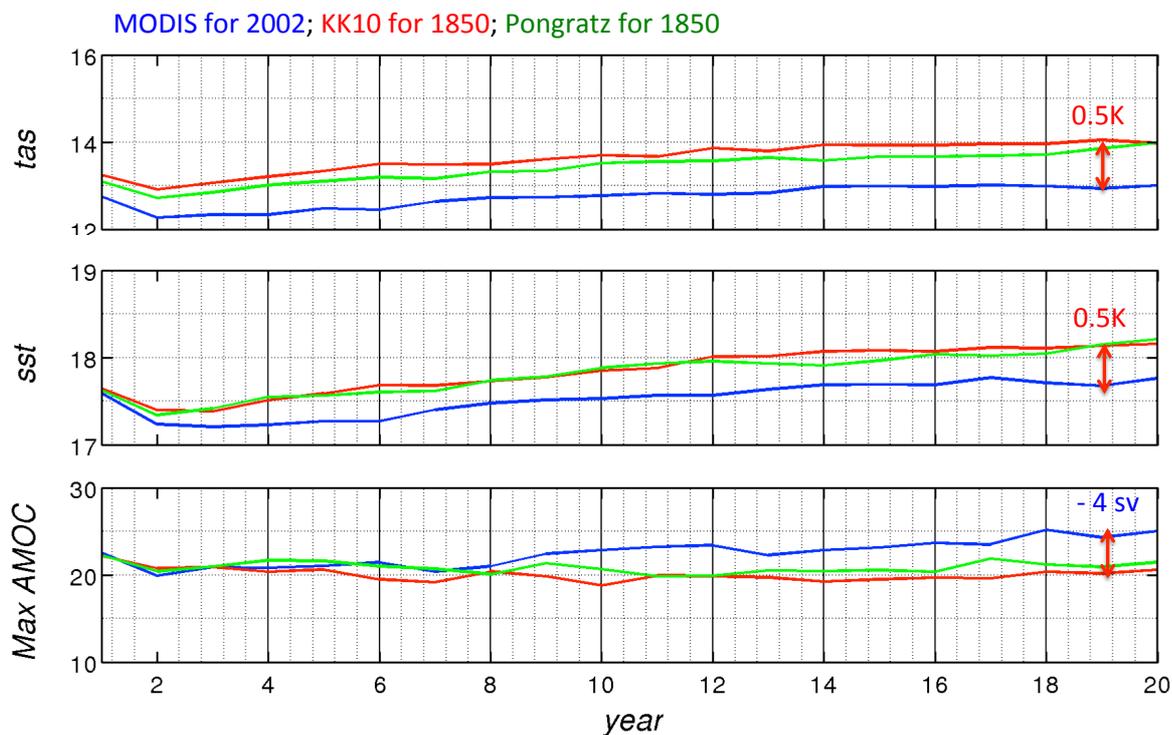
Figure 4. Evolution of global mean surface air temperature, SST and maximum AMOC in 20-year simulations for MODIS albedo, modified albedo corresponding to land-use reconstruction from Pangratz and Kapalan for year 1850 climate condition.

In CMIP5 historical simulations for 1850-2005, the land surface albedo is kept as MODIS value in EC-Earth. It means the effect of land-use change in last 100 years has not been taken into account in EC-Earth simulations. Figure 3 shows that the albedo in large area of continent could be 10 to 20% lower in 1850 than today. If we use the fixed land surface albedo, it would underestimate about 0.5°C of the global mean surface air temperature and SST (Figure 4). With the modified land albedo, global mean SST is about 18°C in 1850 and close to HadiSST data. We also notice a more reasonable maximum Atlantic meridional overturning circulation (AMOC) with 20 SV.

2. Paleo-simulations with EC-Earth

With above implementations in EC-Earth, we have setup several simulations by following PMIP protocol. The boundary conditions have been provided for mid-Holocene (MH, 6 ka), Last Glacial Maximum (LGM, 21 ka) and last millennium (LM, 850-1850 AD), as well as mid-Pliocene (3.2 ma) . For mid-Holocene we set the orbital year as 6000 years before present day and modified the CH4 concentration in forcing file. For LGM, except change the orbital forcing and greenhouse gas, we also modified the ice-sheet extension, topography, coastline and runoff in IFS as well as the bathymetry in ocean model NEMO due to the absence of large area of ice-sheet and 130 metres drop of sea level. For LM, we set yearly varied orbital forcing and we adopted the yearly-varied reconstruction files for volcanic forcing, greenhouse gas concentration, solar radiation, and land-use. For mid-Pliocene, we set the CO_2 level to 400 ppm, and changed few geographical distribution, such as closure of Bering strait.

Several scientific question oriented sensitivity simulations have been run for mid-Holocene and LGM, which are summarized below. Scientific questions are explored by examining the Last millennium and mid-Pliocene model output.

2.1 Green Sahara experiments for mid-Holocene

Paleo-proxy data suggest that one of the most dramatic changes in rainfall over Africa occurred around 15000 years ago, when increased summer precipitations led to an expansion of the North African lakes and wetlands and an extension of grassland and shrubland into areas that are now desert, giving origin to the so-called "Green Sahara", or African Humid Period. However model

This template is available at:
http://www.ecmwf.int/en/computing/access-computing-facilities/forms

simulations have shown limited skill in reproducing the wide range of monsoon amplification responses when forced with Mid-Holocene insolation forcing only. These discrepancies must lie in a shortcoming common to all models such as the improper dust emissions and land surface cover.

With EC-Earth 3.1, we have designed several sensitivity experiments to investigate how potential change in Saharan dust emissions and land surface properties may have altered the climate system in the past. The experiments are listed in table 1.

Table 1. The forcings setup for Green Sahara experiments. The changes in vegetation and dust are applied to the northern African domain 11-33°N, 15°W-35°E.

Experiment	Exp-name	Orbital year	GHG-CH4	Sahara vegetation	Sahara dust
PI control	B400	1850	760	As CMIP5 PI	As CMIP5 PI
6k control	B6KA	- 6000	650	As CMIP5 PI	As CMIP5 PI
6k green dust	G501	- 6000	650	Sahara as shrub	Reduced dust
6k desert dust	P501	- 6000	650	As CMIP5 PI	Reduced dust
PI green	C100	1850	760	Sahara as shrub	As CMIP5 PI
PI green dust	C600	1850	760	Sahara as shrub	Reduced dust
PI desert dust	C700	1850	760	As CMIP5 PI	Reduced dust

The local and remote climate responses based on these experiments have been investigated within the collaboration in Bolin centre where involving PhD student and postdoc fellows, and the results have been published/submitted. Following the review comments on our submitted paper, we have re-run several experiments by using a new dust map that based on satellite data. A few additional experiments have been run upon the suggestions from the reviewers. Three more high-impact articles have been published based on these simulations and more analyses are ongoing by sharing the data within the international project. 6-hourly data from these simulations are provided as boundary conditions to several regional modelling groups. The results also presented in several institutions upon invitation. This work also progressed into a successful research grant funded by Swedish Research Council (See future plan for new application).

The major results from these experiments are:

- We further investigated the mechanisms behind the northward extension of the West African Monsoon during the Mid-Holocene. The results show a substantial modification of the monsoonal circulation, characterized by an intensification of large-scale deep convection through the entire Sahara, and a weakening and northward shift (~6.5°) of the African easterly jet. The greening of the Sahara also leads to a substantial reduction in African easterly wave activity and the associated precipitation. The reorganization of the regional atmospheric circulation is driven by the vegetation effect on radiative forcing and associated heat fluxes, with the reduction in dust concentration to enhance this response. (Pausata et al., 2016; Gaetani et al., 2017)
- We show that accounting for a vegetated and less dusty Sahara during the mid-Holocene relative to preindustrial climate can reduce ENSO variability by 25%, more than twice the decrease obtained using orbital forcing alone. We identify changes in tropical Atlantic mean state and variability caused by the momentous strength- ening of the West Africa Monsoon (WAM) as critical factors in amplifying ENSO's response to insolation forcing through changes in the Walker circulation. Our results thus suggest that potential changes in the WAM due to anthropogenic warming may influence ENSO variability in the future as well. (Pausata et al., 2017a)
- We also show that the greening of the Sahara and reduced dust loadings lead to more favorable conditions for tropical cyclone development compared with the orbital forcing alone. In particular, the strengthening of the West African Monsoon induced by the Sahara greening

This template is available at:
http://www.ecmwf.int/en/computing/access-computing-facilities/forms

triggers a change in atmospheric circulation that affects the entire tropics. Furthermore, whereas previous studies suggest lower TC activity despite stronger summer insolation and warmer sea surface temperature in the Northern Hemi- sphere, accounting for the Sahara greening and reduced dust concentrations leads instead to an increase of TC activity in both hemispheres, particularly over the Caribbean basin and East Coast of North America. Our study highlights the importance of regional changes in land cover and dust concentrations in affecting the potential intensity and genesis of past TCs and suggests that both factors may have appreciable influence on TC activity in a future warmer climate. Through the publications and presentations of these scientific results, we have seen that more interests are drawn to these Green Sahara experiments and more investigations can be established within collaboration. (Pausata et al., 2017b)

2.2 Different initial conditions for LGM simulation

We have performed two time slice last glacial maximum (LGM) simulations starting from different ocean initial conditions. Both initial conditions are taken from previous LGM runs by Zhang et al (2013) and interpolated to the present numerical grid. The two initial ocean states differ by their vertical stratification, and in terms of the vertical profile of the ocean, one initial condition is more like a glacial ocean (hereafter named LGM1 run), while the other is more like a present-day ocean (hereafter named LGM2 run). In Figure 5, the temporal evolutions of the global sea surface temperature from both runs are shown. In addition, a previous control run i.e. pre-industrial (PI) run, is added for comparison. Though we already start simulations by using initial conditions from a previous LGM simulation, and after several hundred years of spin up, the surface temperature still seems not reach a quasi-equilibrium state, indicating the expansive nature of such paleo simulations. The global mean SST in LGM is about 13-14°C and about 3°C less than the PI run.
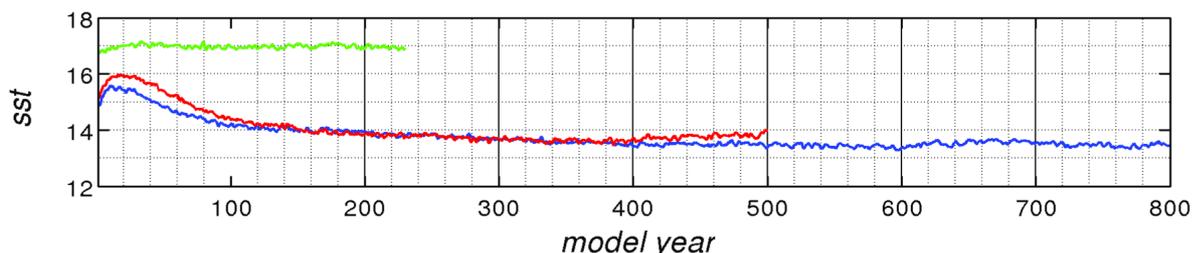

Figure 5. The evolution of global mean sea surface temperature (SST) of two LGM runs and the control run. LGM1 run in blue, LGM2 run in red and PI run in green.

The LGM climate is characterised by not only colder but also drier comparing to present day. This is shown in Figures 6 and 7 where averaging of the last 100 years of 2m air temperature and precipitation comparing with the control run. Figure 6 shows the global 2-metre air temperature of the control run and the difference between the LGM1 run and PI run. Large cooling over the ice sheet is observed while the cooling over the ocean is much smaller. The global averaged value is about 6.6°C lower in LGM1 run than PI run.

The changes of the annual precipitation are shown in Figure 7. For most of the area the precipitation is reduced. Compared to PI run, large decreases of precipitation mainly occur along the coast, e.g. the northwestern coast of north America and west coast of Japan. In the tropical region, slight decrease of the precipitation occurs in the Intertropical convergence zone (ITCZ) which is also consistent with previous studies, see e.g. Toracinta et al 2004. In the South Pacific convergence zone (SPCZ), an increase of the precipitation is observed relative to PI run, and this enhancing of precipitation is also shown in the previous studies and attributed to the difference in surface temperature gradients (Toracinta et al., 2004). For the present LGM runs, the change of precipitation over the ice sheet is marginal, and this is different from a previous LGM run by Otto-Bliesner et al (2006) in which up to 2 mm/day of precipitation decreases over the continental ice sheets are observed.
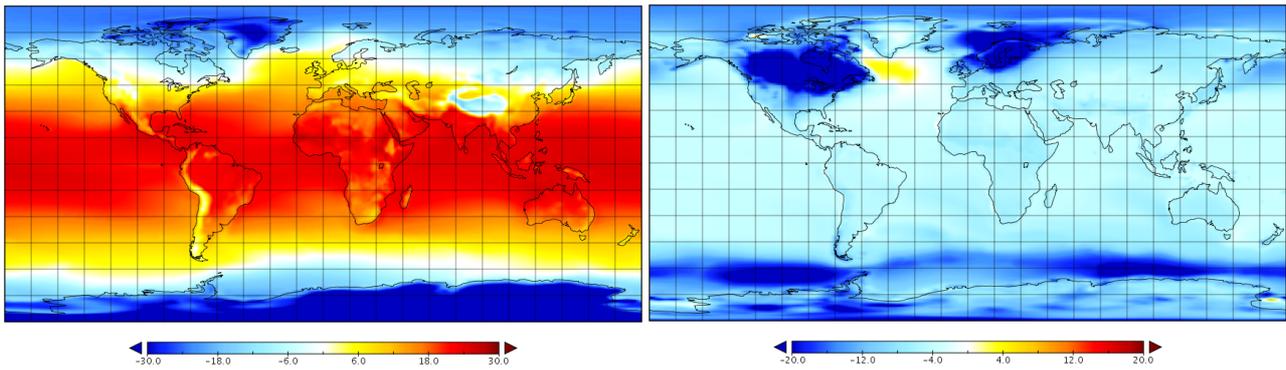
Figure 6. The global 2m air temperature (°C). Left: The PI control run; Right: The difference between the LGM1 run and PI run.
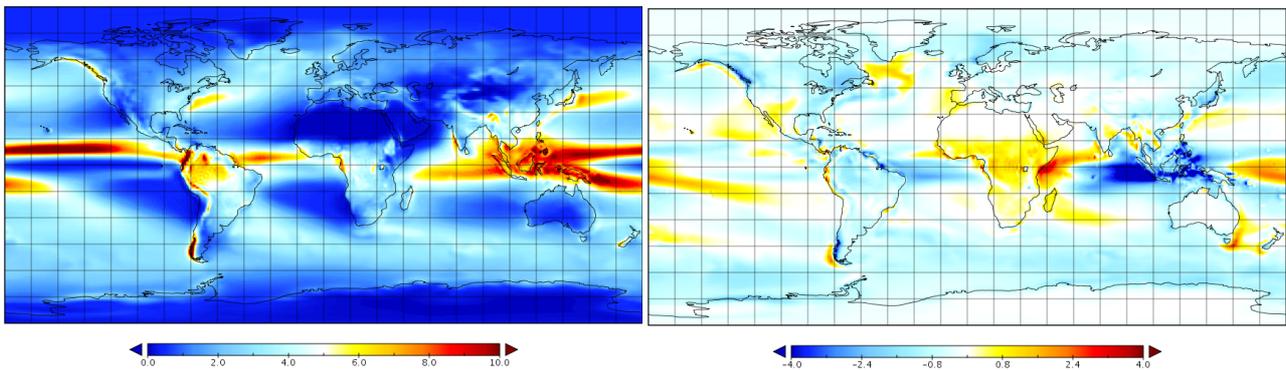

Figure 7. The global precipitation (mm/day). Left: The control run; Right: The difference between the LGM1 and PI run.
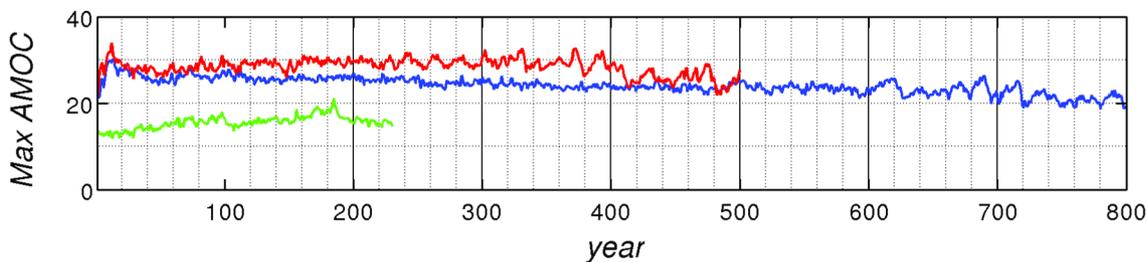

Figure 8. The evolution of AMOC strength of two LGM runs and the control run. LGM1 run in blue, LGM2 run in red and PI run in green.

The Atlantic Meridional Overturning Circulation (AMOC) time series are shown in Figure 8. Though many proxy data suggest a weakening of AMOC strength, the present results are showing an opposite trend. About 20 SV is reached by LGM1 at model year 800 and LGM2 is consistently slightly higher than LGM1 run and reaches about 25 sv at model year 500. These values are consistent with simulation by Zhang et al (2013) and other previous simulations, e.g. see Sueyoshi et al (2013). Note that Weber et al (2007) found that about half of the PMIP2 models have problem simulating a weaker AMOC and due to coarse resolution, non-realistic diffusion coefficients, no consideration of the mixing due to winds and tides. This suggests large sensitivity with respect to the various forcings of AMOC responses and further investigations need to be done to understand the behaviours.

Moreover, in Zhang et al 2013, they observed that after very long integration time, i.e. about 4000 model years, both the two different ocean states reach equilibrium and are stable. Note that in Zhang et al (2013), they use a much coarser horizontal resolution of the ocean which is about 3 °C while the present study is about 1°C. However, our results show that after few hundred years, the

present-day like initial ocean state is unstable and finally both runs becomes a glacial ocean though started differently.

2.3 Regime shift in LGM simulation

As reported previously, our LGM simulation encountered a 'strange' behaviour when model run after 800 years, the sea ice grows exponentially. During the year we have discussed with many oceanographers, sea ice experts and modelers, try to understand if it is a model technical problem or a naturally variability in the model system. It is difficult to explain the sea ice growth, in particular after around year 600 when the growth rate accelerates in an exponential manner. If the growth was thermodynamic, the growth rate would decrease with time — not increase. The thermodynamic growth of 100–200 m ice is very weak and cannot physically explain what happens. Surface accumulation of snow also could not give an accelerated growth. Most modeling groups that run LGM simulations did not report such problem because they either did not run more than 500 years, or they have the constrain of sea ice growth, such as a CCSM LGM simulation "In the glacial model runs, the potential mean sea-ice thickness of each grid cell is limited to a maximum of 30 m in order to reach equilibrium." As showing in Figure 9, a continuous run does tend to a decrease in sea-ice growth and global mean sea surface temperature increase, which indicating a climate regime shift to another equilibrium state. This problem is expected to be solved with new ocean and sea-ice model version.
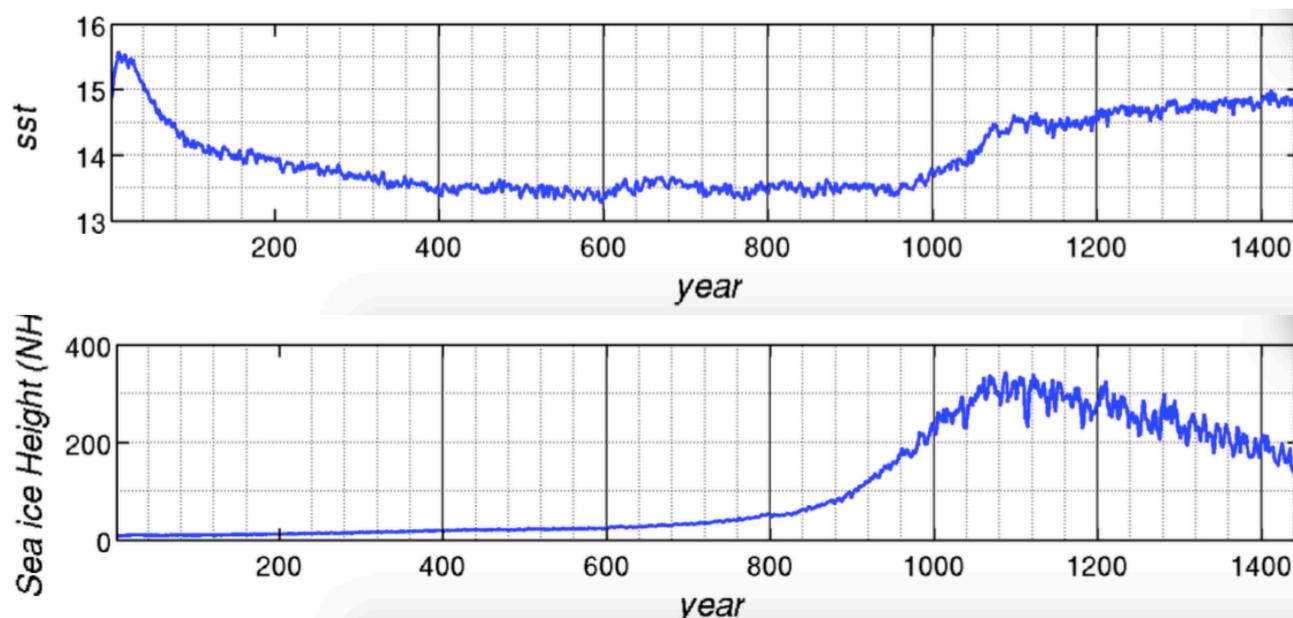

Figure 9. The evolution of global mean sea surface temperature (SST) and sea ice thickness in Northern Hemisphere in LGM run for 1450 years.

2.4 Testing of different ice-sheet boundary conditions for LGM simulation

In previous PMIP3 LGM protocol, an ice-sheet reconstruction is given for all the modelling groups. In upcoming PMIP4 LGM protocol, the previous ice-sheet reconstruction is no longer recommended but provides two new ice sheet reconstructions by Peltier et al. (2015) and Tarasov et al. (2002, 2012). To compare how sensitive the model to these boundary conditions, we have used all provided ice-sheet and did the test runs under LGM condition. All the runs are started from 300 years of previous run and a comparison in global mean SST shows that those new ice sheet reconstructions are about 0.5°C warmer than the previous PMIP3 boundary condition. SST from Peltier reconstruction is a bit warmer than those from Tarasov.
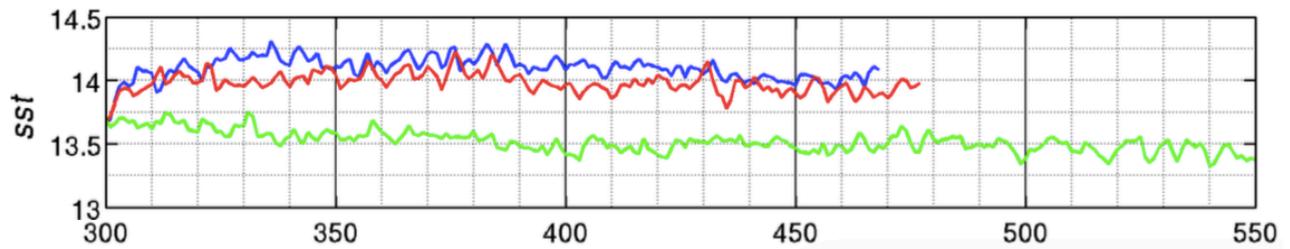
Figure 10. The evolution of global mean SST in LGM runs with three ice-sheet reconstructions, blue: Dick Peltier, red: Lev Tarasov, and green: PMIP3.

2.5 Multi-decadal rainfall variability in Western Africa during last millennium

We have analysed multi-decadal rainfall variability over West Africa using our last millennium simulation with EC-Earth. Our model results show an overall drying trend during last millennium, characterized with wet condition during the Medieval Warm Period and dry condition during Little Ice Age (fig 3), especially in the Sahel region. These features are mostly due to the external forcing such as the changes in solar radiation and volcanic eruptions. By removing the linear trend caused by external forcing, we found that high decadal variability in rainfall over the Coast of Guinea, which is modulated by the tropical Atlantic SST. While the rainfall variability over the Sahel region exhibits strong multidecadal variability, which is closely connected to Atlantic multidecadal variability. (Zhang et al., manuscript in preparing)
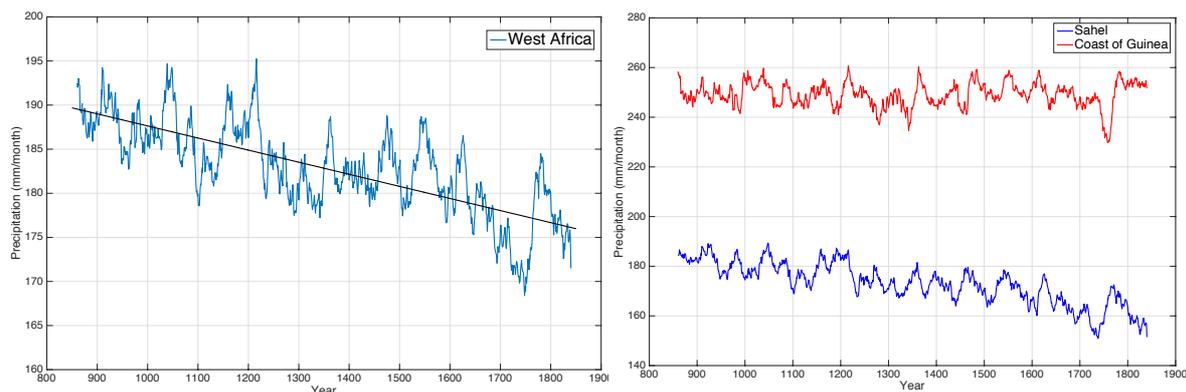

Figure 11. The evolution of summer rainfall (unit: mm/month) during last millennium over (a) western Africa and (b) Sahel (blue) and Coast of Guinea (red).

2.6 Arctic amplification in Mid-Pliocene simulation

Another focus during this year is the simulation for mid-Pliocene. We have identified some problems in previous finished Mid-Pliocene experiment with EC-Earth 3.1, where we found some weird character in AMOC, which may be caused by the incorrect modification of topography. We have to carefully setup the experiment with correct topography and ocean bathymetric and re-run the simulation. Our second Pliocene experiment shows the similar results as in first simulation but has more sea-ice in Arctic and no ice-free summer is exhibited. We have focused on investing the Arctic amplification in this simulation. A quantification of process contribution using the Climate Feedback and Response Analysis Method (CFRAM) shows that the largest contributor to Arctic amplification is sea-ice albedo feedback and cloud feedback plays a secondary role, whereas the latent and sensible heat fluxes largely offset Arctic amplification through a negative feedback (Fig 12). Significant sea-ice melting is found during summer months from June to October. The large area of open-water facilitates oceanic dynamical process to store large amount of heat content in the ocean. The stored energy is discharged in winter to sea surface, heats the overlying atmosphere through turbulent heat fluxes, and thus maintains the more pronounced Arctic amplification in winter in spite of no incoming solar radiation during polar night. (Zheng et al., submitted)
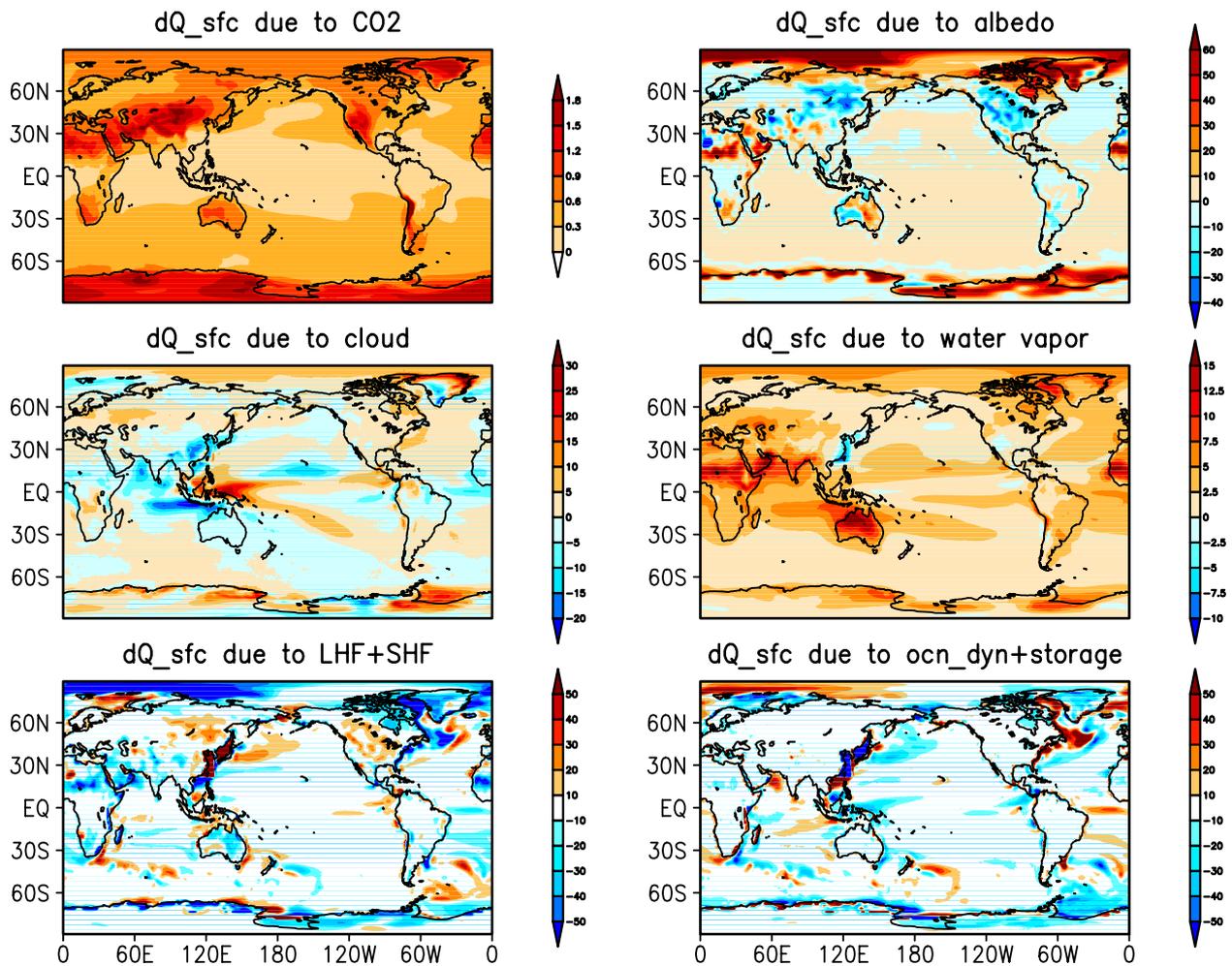
Figure 12. Partial surface temperature changes attributable to radiative processes CO2 forcing, albedo feedback, cloud feedback, water vapor feedback, surface tube turbulence feedback, and ocean dynamic feedback.

We also found that the spatial variation of sea surface temperate (SST) plays a vital role in regulating climate change. Most of previous studies on formation of SST pattern have focused on low and middle latitudes, which involving strong air-sea interaction. However, in high latitudes such as Arctic Ocean, air-sea-ice interaction has to be considered due to the present of sea-ice. The geological data indicate substantial warming over north Atlantic during the Pliocene. However, most climate models underestimate this character in their Pliocene simulations. Our EC-Earth simulation does show pronounced warming SST over North Atlantic in particular over Greenland Sea and Baffin Bay, which is comparable with geological reconstructions. We identify this anomalous warming pattern is the synthesis of SST change in different season. The strongest warming is exhibited in winter in surface air temperature (SAT) over the Arctic Ocean around North Pole, while the change in SST is not evident here due to lack of ocean-atmosphere coupling because of the isolating effect of sea-ice. In summer the warming in SAT is prominent over Greenland Sea and Baffin Bay because of strong ice-albedo positive feedback in ice-melting season, and thus lead to the SST warming through the atmospheric forcing to ocean.

List of publications/reports from the project with complete references

1. **Zhang Q**., J.C. Hargreaves, P. Braconnot and M. Kageyama, 2017: PMIP4 contribution to CMIP6, PAGES magezine, 25, 160, https://doi.org/10.22498/pages.25.3.160.

2. An, W., S. Hou, **Q. Zhang**, W. Zhang, S. Wu, H. Xu, H. Pang, Y. Wang, and Y. Liu, 2017: Enhanced recent local moisture recycling on the northwestern Tibetan Plateau deduced from ice core deuterium excess records. Journal of Geophysical Research: Atmospheres, 122. https://doi.org/10.1002/2017JD027235.

3. Kageyama, M., Albani, S., Braconnot, P., Harrison, S. P., Hopcroft, P. O., Ivanovic, R. F., Lambert, F., Marti, O., Peltier, W. R., Peterschmitt, J.-Y., Roche, D. M., Tarasov, L., Zhang, X., Brady, E. C., Haywood, A. M., LeGrande, A. N., Lunt, D. J., Mahowald, N. M., Mikolajewicz, U., Nisancioglu, K. H., Otto-Bliesner, B. L., Renssen, H., Tomas, R. A., **Zhang, Q**., Abe-Ouchi, A., Bartlein, P. J., Cao, J., Li, Q., Lohmann, G., Ohgaito, R., Shi, X., Volodin, E., Yoshida, K., Zhang, X., and Zheng, W.: The PMIP4 contribution to CMIP6 – Part 4: Scientific objectives and experimental design of the PMIP4-CMIP6 Last Glacial Maximum experiments and PMIP4 sensitivity experiments, Geosci. Model Dev., 10, 4035-4055, https://doi.org/10.5194/gmd-10-4035-2017, 2017.

4. Jungclaus, J. H., Bard, E., Baroni, M., Braconnot, P., Cao, J., Chini, L. P., Egorova, T., Evans, M., González-Rouco, J. F., Goosse, H., Hurtt, G. C., Joos, F., Kaplan, J. O., Khodri, M., Klein Goldewijk, K., Krivova, N., LeGrande, A. N., Lorenz, S. J., Luterbacher, J., Man, W., Maycock, A. C., Meinshausen, M., Moberg, A., Muscheler, R., Nehrbass-Ahles, C., Otto-Bliesner, B. I., Phipps, S. J., Pongratz, J., Rozanov, E., Schmidt, G. A., Schmidt, H., Schmutz, W., Schurer, A., Shapiro, A. I., Sigl, M., Smerdon, J. E., Solanki, S. K., Timmreck, C., Toohey, M., Usoskin, I. G., Wagner, S., Wu, C.-J., Yeo, K. L., Zanchettin, D., **Zhang, Q**., and Zorita, E.: The PMIP4 contribution to CMIP6 – Part 3: The last millennium, scientific objective, and experimental design for the PMIP4 *past1000* simulations, Geosci. Model Dev., 10, 4005-4033, https://doi.org/10.5194/gmd-10-4005-2017, 2017.

5. Otto-Bliesner, B. L., Braconnot, P., Harrison, S. P., Lunt, D. J., Abe-Ouchi, A., Albani, S., Bartlein, P. J., Capron, E., Carlson, A. E., Dutton, A., Fischer, H., Goelzer, H., Govin, A., Haywood, A., Joos, F., LeGrande, A. N., Lipscomb, W. H., Lohmann, G., Mahowald, N., Nehrbass-Ahles, C., Pausata, F. S. R., Peterschmitt, J.-Y., Phipps, S. J., Renssen, H., and **Zhang, Q**.: The PMIP4 contribution to CMIP6 – Part 2: Two interglacials, scientific objective and experimental design for Holocene and Last Interglacial simulations, Geosci. Model Dev., 10, 3979-4003, https://doi.org/10.5194/gmd-10-3979-2017, 2017.

6. Helsen, M. M., W. van de Wal, R. S. W., Reerink, T. J., Bintanja, R., Madsen, M. S., Yang, S., Li, Q., and **Zhang, Q**., 2017: On the importance of the albedo parameterization for the mass balance of the Greenland ice sheet in EC-Earth, The Cryosphere, 11, 1949-1965, https://doi.org/10.5194/tc-11-1949-2017.

7. Pausata, F. S., **Q. Zhang**, F. Mischitiello, Z. Lu, L. Chafik, E. M. Niedermeyer, J. C. Stager, K. M. Cobb, and Z. Liu, 2017: Greening of the Sahara suppressed ENSO activity during the mid-Holocene. *Nature Communications*, **8**.

8. Gaetani, M., G. Messori, **Q. Zhang**, C. Flamant, and F.S. Pausata, 2017: Understanding the mechanisms behind the northward extension of the West African Monsoon during the Mid-Holocene. J. Climate, https://doi.org/10.1175/JCLI-D-16-0299.1

9. Pausata, F. S. R., K. A. Emanuel, M. Chiacchio, G. T. Diro, **Q. Zhang**, L. Sushama, J. C. Stager, and J. P. Donnelly. 2017. Tropical cyclone activity enhanced by Sahara greening and reduced dust emissions during the African Humid Period. Proceedings of the National Academy of Sciences.

10. Hind, A., **Q. Zhang** and G. Brattström, 2016: Problems encountered when defining Arctic amplification as a ratio. *Sci. Rep.* 6, 30469; doi: 10.1038/srep30469.

11. Salih, A. A. M., **Q. Zhang**, F. S. R. Pausata, and M. Tjernström, 2016: Sources of Sahelian-Sudan moisture: Insights from a moisture-tracing atmospheric model, J. Geophys. Res. Atmos., 121, 7819–7832, doi:10.1002/2015JD024575.

12. Pausata, F.S.R., G. Messori and **Q. Zhang**, 2016: Impacts of dust reduction on the northward expansion of the African monsoon during the Green Sahara period, Earth and Planetary Science Letters, 434, 298-307, doi:10.1016/j.epsl.2015.11.04.

13. Zhang, P., D. Chen, H.W. Linderholm, **Q. Zhang**, 2015: How similar are annual and summer temperature variability in central Sweden?, Advances in Climate Change Research, 6, 159-170, doi: 10.1016/j.accre.2015.11.001.

14. Yang, H., Y. Zhao, Z. Liu, Q. Li, F. He and **Q. Zhang**, 2015: Heat Transport Compensation in Atmosphere and Ocean over the Past 22,000 Years. *Sci. Rep.*, 5, 16661, doi: 10.1038/srep16661.

15. Muschitiello, F., **Q. Zhang**, H. S. Sundqvist, F. J. Davies, and H. Renssen, 2015: Arctic climate response to the termination of the African Humid Period. Quaternary Science Reviews, 125, 91-97, doi:10.1016/j.quascirev.2015.08.012.

16. Ballarotta, M., R. Fabien, S. Falahat, **Q. Zhang** and G. Madec, 2015: Impact of the oceanic geothermal heat flux on a glacial ocean state, Clim. Past Discuss., 11, 3597-3624, doi:10.5194/cpd-11-3597-2015.

17. Xu, G., X. Liu, G. Wu, T. Chen, W. Wang, **Q. Zhang**, Y. Zhang, X. Zeng, D. Qin, W. Sun, and X. Zhang, 2015: Tree ring δ18O's indication of a shift to a wetter climate since the 1880s in the western Tianshan Mountains of northwestern China. J. Geophys. Res. Atmos., 120, 6409–6425. doi: 10.1002/2014JD023027.
18. Salih, A. A. M., **Q. Zhang**, and M. Tjernström, 2015: Lagrangian tracing of Sahelian Sudan moisture sources, J. Geophys. Res. Atmos., 120, 6793–6808, doi:10.1002/ 2015JD023238.
19. **Zhang, Q.**, Holmgren, K., and Sundqvist, H. S., 2015: Decadal Rainfall Dipole Oscillation over Southern Africa Modulated by Variation of Austral Summer Land–Sea Contrast along the East Coast of Africa. *J. Atmos. Sci.*, **72**, 1827–1836. doi: http://dx.doi.org/10.1175/JAS-D-14-0079.1

Future plans

(Please let us know of any imminent plans regarding a continuation of this research activity, in particular if they are linked to another/new Special Project.)

1. Within a research grant "Simulating the green Sahara with an Earth System Model" (2018-2021) we will continue to investigate the mechanism for abrupt collapse of Saharan vegetation during mid-Holocene. The project will be based on a thousands years transient simulation which demands heavy computation. We submitted a new application for HPC resource from ECMWF for 2019-2021, hopefully will be granted.
2. We have committed to run five Tire 1 PMIP4 experiments in CMIP6, these simulations will be run on NSC HPC resources in Sweden.
3. We are working on the implementation of stable water isotope into OpenIFS. This implementation will facilitate the study on hydrological cycle in the atmosphere, benefit both the present day and past climate change research. The coding and testing work right now do not require too much HPC, once the implementation is completed, we may apply for extra resource for stable water isotope modelling.